Journal of Materials Science and Chemical Engineering, 2026, 14(5), 36-46
https://www.scirp.org/journal/msce
ISSN Online: 2327-6053
ISSN Print: 2327-6045

Corrosion Resistance of Stamped Al Alloy 6451 with PEO Coating

Yuanming Zheng, Zihan Zhou, Jairui Li, Tianyi Zhang, Wutian Shen, Peilin Ying, Henry Hu*, Xueyuan Nie

Department of Mechanical, Automotive & Materials Engineering University of Windsor, Windsor, Canada
Email: zheng1q@uwindsor.ca, zhou18m@uwindsor.ca, lijiaru@uwindsor.ca, zhang4x3@uwindsor.ca, shen12a@uwindsor.ca, yingp@uwindsor.ca, *huh@uwindsor.ca, xnie@uwindsor.ca

How to cite this paper: Zheng, Y.M., Zhou, Z.H., Li, J.R., Zhang, T.Y., Shen, W.T., Ying, P.L., Hu, H. and Nie, X.Y. (2026) Corrosion Resistance of Stamped Al Alloy 6451 with PEO Coating. *Journal of Materials Science and Chemical Engineering*, **14**, 36-46.
https://doi.org/10.4236/msce.2026.145004

Received: March 26, 2026
Accepted: May 25, 2026
Published: May 28, 2026

Abstract

Recently, stamped wrought Al alloy 6451 is implemented to produce automotive enclosures such as tailgates, which often suffer harsh environment during service. The corrosion resistance of Al alloy 6451 needs to be improved essentially. In this study, oxide coatings were applied on stamped wrought Al 6451 with the help of Plasma Electrolytic Oxidation (PEO) technique to enhance its corrosion resistance. A potentiodynamic polarization test was conducted to investigate corrosion resistances of uncoated and coated samples. The results of the potentiodynamic polarization tests revealed that the corrosion resistances of uncoated, thin-coated, and thick-coated Al 6451 samples were 7282.5 $\Omega \cdot cm^2$, 11583.3 $\Omega \cdot cm^2$, and 41,151 $\Omega \cdot cm^2$, respectively. These findings clearly demonstrate that the growth of the coating layer significantly enhances the substrate's ability to withstand corrosive environments. Scanning Electron Microscopy (SEM) and Energy Dispersive X-ray (EDX) were employed to investigate the variation of surface morphologies and chemical composition of the PEO coatings. The SEM observation indicated that the coating layers exhibited a smooth surface compared to the as-coated condition, and pitting corrosion occurred on the corroded coating surfaces. The EDX spectra showed a reduction in the calculated Al/Si intensity ratio before and after the corrosion tests.

Keywords

Al Alloy 6451, PEO Coating, Corrosion Resistance, Surface Characterization

1. Introduction

Over the past two decades, innovations in automotive technology have led to a

20% increase in vehicle horsepower and a 32% improvement in average new vehicle fuel economy. However, CO_2 emissions have risen by 5%, primarily due to a 4% increase in average vehicle weight [1] [2]. This weight gain is largely attributed to consumer demand for enhanced safety, comfort, and convenience, which requires the integration of safety-oriented technologies (e.g., anti-lock braking systems, electronic stability control, tire pressure monitoring systems) and structural components (e.g., airbags, laminated glass, door intrusion beams) [2]. Moreover, emerging battery-powered electric vehicles (BEVs) are, on average, approximately 30% heavier than traditional gasoline or diesel-powered vehicles (GDVs) [3]-[5]. Consequently, reducing vehicle weight is critical for lowering emissions in GDVs and improving energy efficiency and driving range in BEVs. In response to these challenges, the automotive industry has shifted from all-steel body structures to mixed-material architectures to improve weight efficiency. Aluminum offers several advantages: its density is about one-third that of steel, its melting point (~600˚C) is significantly lower than that of steel (~1500˚C), allowing for energy-efficient processing, and it is more cost-effective for casting and fabrication [6]. Notable milestones include the introduction of aluminum-intensive vehicles such as the Acura NSX and Jaguar XJ in the 1990s, enabled by the development of specialized cast aluminum alloys. In 2013, GM introduced its first cast aluminum shock tower in the Cadillac ATS, achieving a 50% weight reduction; the component weighed only 2.8 kg [7] [8]. Although aluminum has lower surface hardness than steel, this limitation can be mitigated through surface coatings [9]. Additionally, aluminum alloys can achieve tensile strengths up to 700 MPa depending on their composition. These attributes make aluminum alloys highly attractive for automotive closures due to their lightweight nature compared to steel [7] [10].

Generally, aluminum alloys exhibit good atmospheric corrosion resistance. However, their corrosion resistance in aqueous environments is often poor. Corrosion in aluminum alloys is driven by the interaction between localized cathodic/anodic sites and the alloy matrix, resulting in various forms of degradation such as pitting, selective dissolution, trenching, intermetallic particle etch-out, intergranular attack, and exfoliation corrosion [11]-[13]. Aluminum is unique in exhibiting both high reactivity and passivity. It readily reacts with oxygen and water to form a coherent, protective oxide layer that inhibits further corrosion. Unlike rust on steel, aluminum oxide does not flake off and is considerably harder, forming a stable white surface that regenerates if scratched or abraded [14] [15]. The 6xxx series Al alloys, which contain Si and Mg, demonstrate appreciable corrosion resistance and immunity to stress corrosion cracking. The presence of both Mg and Si leads to the formation of Mg_2Si precipitates, which are anodic relative to the Al matrix and thus susceptible to selective dissolution. An excess of Si can exacerbate corrosion by increasing cathodic reaction rates and promoting intergranular corrosion due to Si enrichment at grain boundaries [12]. Lately, stamped wrought Al alloy 6451, which contains both Si and Mg, has been increasingly used

in the production of automotive enclosures such as tailgates. These components are often exposed to harsh environmental conditions during service, making corrosion resistance a critical concern for their engineering performance. Therefore, enhancing the corrosion resistance of Al alloy 6451 is essential to ensure long-term durability and performance [16].

Plasma electrolytic oxidation is an emerging surface treatment which was developed with the purpose of combating corrosion on Al and Mg-based light alloys. The process produces thick, dense, ceramic-like metal oxide coating layers on the surface of Al, Mg and Ti alloys, significantly improving the wear and corrosion resistance of the substrate. The process could be termed as micro-arc oxidation (MAO), plasma chemical oxidation (PCO) or anodic oxidation by spark discharge [17]. PEO process employs weak alkaline which is environmentally friendly as electrolyte, and then immerse the substrate in the bath and let high electric voltages pass through, the oxidation layer initiates simply. The thickness of the oxide coating grows during the process in the range of a few microns up to hundreds of microns based on the properties of the substrate. The PEO coating process has been extensively involved in research for a long period of time, in the fields of automobile, biomedical, aerospace and electronic applications, and competed with other conventional surface treatment methods. Compared to conventional surface treatment methods, which incorporate chemical conversion coating, anodizing, electroless/electroplating, organic coating, laser surface treatment, physical vapor deposition (PVD), chemical vapor deposition (CVD) and thermal/cold spray [18], PEO coating process is more environmentally friendly due to the involvement of weak alkaline only. Furthermore, the coating layer does not require appropriate care and control during the operation, since the coating process is continuous as long as there is electric current passing through the substrate.

Despite the long-standing use of aluminum alloys as steel substitutes, limited research exists on the effect of PEO coating on corrosion resistance of stamped wrought Al alloy 6451. In this work, the PEO technique was employed to deposit ceramic coatings on Al alloy 6451 substrates with the help of an AC power supply. A potentiodynamic polarization test was performed to evaluate the corrosion resistance of both uncoated and coated samples. Scanning Electron Microscopy (SEM) and Energy Dispersive X-ray Spectroscopy (EDS) were utilized to examine the surface morphology and analyze the chemical composition of the Plasma Electrolytic Oxidation (PEO) coatings. The coating thicknesses were measured using a coating thickness gauge follow.

2. Experimental Procedures

A Body-In-White (BIW) tailgate from an electric vehicle which was made of Al alloy 6451 was selected as the experimental subject in this study in order to minimize the differences resulted from the variation in composition and microstructures among samples. The BIW tailgate was sectioned in half by waterjet cut and

then saw cut the exterior panel on the tailgate into square pieces with dimensions of 5 mm × 5 mm × 1 mm. After polishing successively on silicon carbide (SiC) sandpaper, followed by cleaning with ethanol and acetone, the samples for coating were stored in UV free secador. The coating thickness was measured by Positector 6000 Series Coating Thickness Gauge. A Mitutoyo surface profiler SJ201P was used to measure the roughness of the PEO coatings. The PEO process was set up with the preparation of the electrolytes. Solutions of Sodium Metasilicate (Na_2SiO_3) (1 - 20 g/l) in distilled water with addition of Potassium Hydroxide (KOH) (0.1 - 5 g/l) were mixed to adjust the pH to 13 and conductivity. During coating deposition, the samples to be coated were treated as anode and the nozzle was as cathode with setup voltage 510 V and current 15 A supplied by AC power source. The coating duration for thin-coated and thick-coated samples were 30 s and 90 s, respectively. ASTM standard A1093/A1093M - 15 (2020) was adopted to conform with the customarily adopted procedures [19]. The potentiodynamic polarization tests were carried out by EC-LAB SP-150 electrochemical apparatus with corrosion analysis EC-LAB software at room temperature (298 K). A three-electrode cell with samples as the working anode, Ag/AgCl sat KCl as the reference electrode, and a platinum rod as counter electrode was utilized during the corrosion tests. The ratio of volume of 3.5 wt% NaCl solution to the surface area of the samples was 350 ml/cm^2. Potentiodynamic polarization scans were conducted at a rate of 10 mV/s from −0.5 V versus open circuit potential in a more noble direction up to 0.5 V versus the reference electrode. At the beginning of the corrosion testing, the samples were grounded with SiC paper with fine grade and held in a salt solution allowing the open circuit potential to settle to a constant value. Scanning Electron Microscopy (SEM) and Energy Dispersive X-ray Analysis (EDX) were utilized to study the surface morphologies and microstructures of samples before and after corrosion tests.

3. Results and Discussion

3.1. Corrosion Tests

Figure 1 shows the polarization curves of uncoated, thin-coated and thick-coated samples. The uncoated sample prepared with sodium metasilicate and potassium hydroxide solutions had a more positive corrosion potential (−576.4 mV) (Curve 1) than that of the thin-coated sample (−598.3 mV) (Curve 2) and that of the thick-coated sample (−616.7 mV) (Curve 3). The corrosion current density for the thick-coated sample 3 (1.3 μA/cm^2) was significantly lower than that of the thin-coated sample (6.1 μA/cm^2) and that of the uncoated sample (11.1 μA/cm^2), which indicates the longer PEO treatment duration, the more completely dense protective coating films formed. The corrosion potentials (E_{corr}), corrosion current density (i_{corr}) and anodic/cathodic Tafel slopes (b_a and b_c) were derived from the test data. Based on the approximately linear polarization at the corrosion potential (E_{corr}), the corrosion resistance (Rp) values were determined from the relationship [20] [21]:

$$R_p = \frac{b_a \times b_c}{2.3 \times i_{corr} \times (b_a + b_c)} \quad (1)$$

A summary of the results of the potentiodynamic corrosion tests is given in **Table 1**. The data revealed the enhanced corrosion protection afforded by the coating layers with different thickness. The two coated samples showed a higher corrosion resistance than the uncoated sample. The coating layer with the PEO treatment duration of 90 s had the best corrosion resistance (41151.0 Ω·cm^2) of all the tested samples. Compared to the uncoated sample, the corrosion potential (E_{corr}) of the thin-coated and thick-coated samples increased by 21.9 mV and 40.3 mV, respectively; and corrosion resistance (R_p) increased by 4300.8 Ω·cm^2 and 33868.5 Ω·cm^2, respectively, while the corrosion current density (i_{corr}) decreased by almost 2 times and one order of magnitude (**Table 1**), respectively.

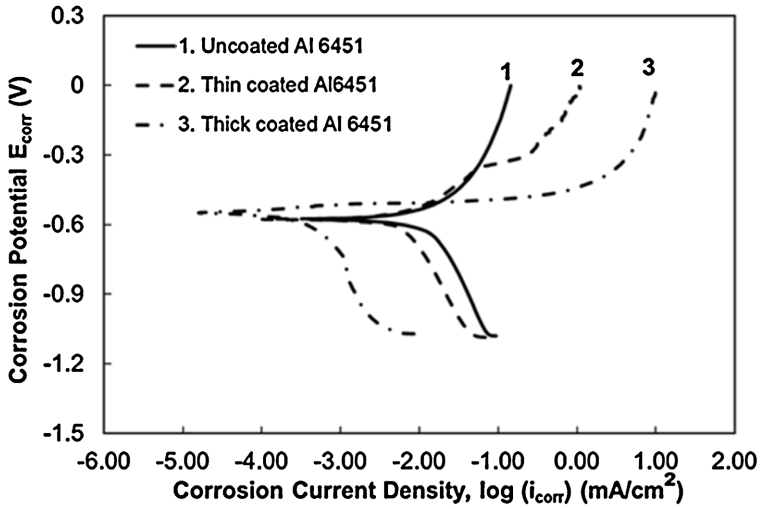

Figure 1. Potentiodynamic polarization curves of uncoated, thin-coated and thick-coated Al 6451.

Table 1. Results of potentiodynamic corrosion tests in 3.5 wt% NaCl solution.

Material	E_{corr} (mV)	I_{corr} (μA)	b_c (mV)	b_a (mV)	R_p (Ω·cm^2)
Uncoated Al 6451	−576.4	11.1	493.5	299.0	7282.5
Thin-coated Al 6451	−598.3	6.1	484.6	245.6	11,583.3
Thick-coated Al 6451	−616.7	1.3	187.9	332.9	41,151.0

Furthermore, large pitting corrosion craters could be observed by naked eye on the uncoated Al alloy 6451 after corrosion tests. The crates resulted from the fact that the corrosion resistance of the uncoated alloy was considerably reduced after the thin, naturally generated protective alumina oxide film on the surface of the uncoated sample dissolved during the corrosion propagation. In addition, the results showed that the PEO coating duration affected the corrosion performance of the stamped wrought Al alloy 6451. With the same electrical process parameters,

the coating generated with the extended PEO processing time of 90 seconds had almost 4 times better corrosion resistance than the one with the PEO duration of 30 seconds

3.2. SEM and EDS Analyses

Figure 2 shows the micrograph of the cross-sections of the interface between the PEO coating layer and the substrate. The thicknesses of the PEO coating layers were measured under SEM and verified by Positector 6000 Series Coating Thickness Gauge, which was 3 μm for thin-coated sample and 10 μm for thick-coated sample. The thin coating was nonuniform and had the thickness variation, which might result from the unevenly distributed spark discharges during the PEO process. In the thick areas, the sparks were concentrated and large, while the sparks were less intensive in the thin coating area leading to a nonuniform growth on the substrate surface. It could be seen that the thick coating regions were thicker than the thin areas in two growth modes. The coating grew inward to its substrate and outward to its external surface.

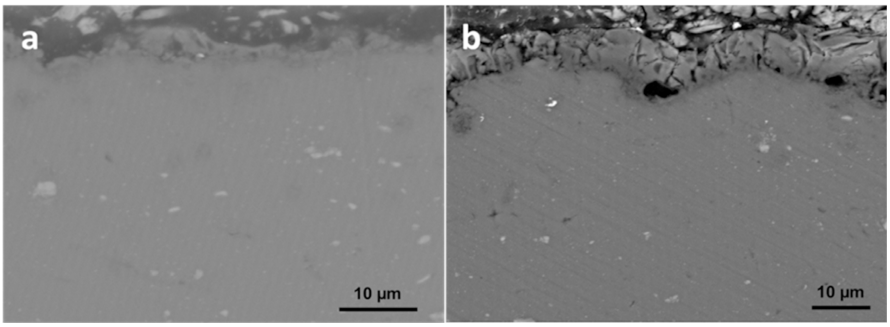

Figure 2. Cross-section of coating layer and substrate, (a) thin-coated and (b) thick-coated Al-6451.

Figure 3 shows the surface morphology of the uncoated Al 6451 before and after corrosion. It appeared that the substrate changed its surface morphology as the corrosion proceeded. Before the corrosion test, the substrate was quite smooth and consistent as displayed in **Figure 3(a)**. The corrosion process resulted in the loss of the thin, naturally formed protective aluminum oxide film, which caused localized corrosion pits as shown by the presence of some dark gray areas in **Figure 3(b)**. This was because the corrosion resistance of the substrate was relatively low.

Figure 4 gives SEM images showing the surface morphology of the thin coating before and after corrosion tests. The overall surface of the thin-coated sample appeared presence of patches and pinholes on the as-coated surface shown in **Figure 4(a)**, which resulted in non-consistent coating layer shown in **Figure 2(a)**. The surface morphology of the thick-coated Al 6451 before and after was depicted in **Figure 5**. The sample with the thick coating displayed scattered fine holes and microcracks in the coating as shown in **Figure 5(a)**. Th presence of the pinholes was caused by the sparks to breakdown the high impedance of both the thick and

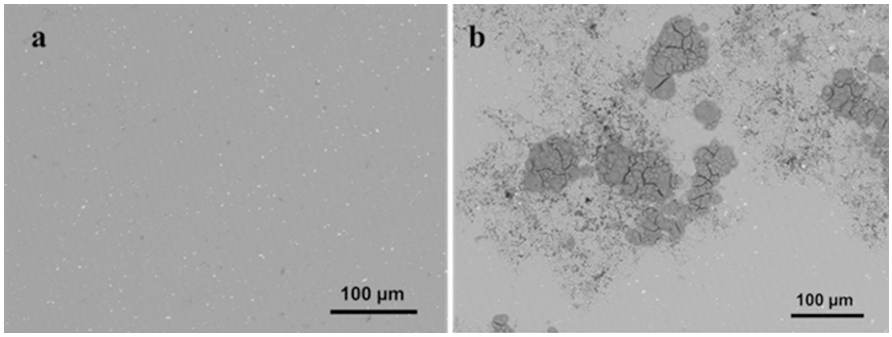

Figure 3. Surface morphology of uncoated Al 6451 (a) before and (b) after corrosion.

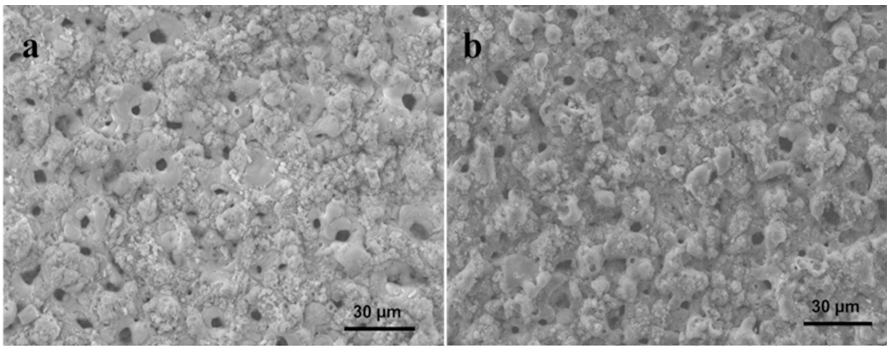

Figure 4. Surface morphology of thin-coated Al 6451 (a) before and (b) after corrosion.

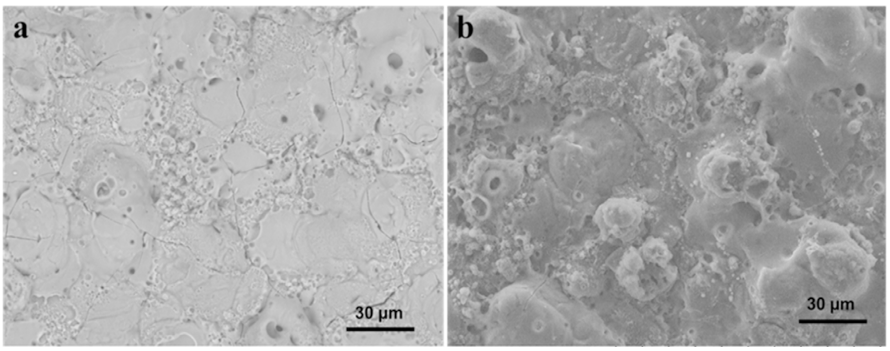

Figure 5. Surface morphology of thick-coated Al 6451 (a) before and (b) after corrosion.

thin coatings. The microcrack formation might result from thermal stresses during the progression of the coating, in which rapid melting and solidification of ceramic compounds such as aluminum oxide took place. They could affect the load-carrying capacity and the durability of the solution. The roughness measurements indicated that the roughnesses (Ra) of the thin-coated and thick-coated samples reduced from 1.47 and 3.03 before the corrosion tests down to 1.33 and 2.88 after the tests. After the corrosion test, the coating layers became smoother than the as-coated surfaces, indicating an electrochemical polishing behavior. Also, it was observed that the pitting corrosion took placed on the corroded coating surfaces due to the presence of the corrosive NaCl solution during the corrosion test.

Figure 6 shows the EDX spectra on surface of the uncoated Al 6451 before and

after corrosion. Oxygen and chlorine were detected by EDX on the corroded surface due to the employment of the NaCl solution during the potentiodynamic polarization tests. The EDX spectra on surface of the thin-coated and thick-coated Al 6451 before and after corrosion are given in **Figure 7** and **Figure 8** respectively. The elements of K, O, Na, Al, Si were detected by EDX on the uncorroded surfaces, which indicated the presence of the PEO coating, since the electrolytes contained the solution of sodium metasilicate (Na_2SiO_3) with addition of potassium hydroxide (KOH). After the corrosion tests, Cl was detected in both coatings. It was worth noting that the relative Si content in the coating appeared to

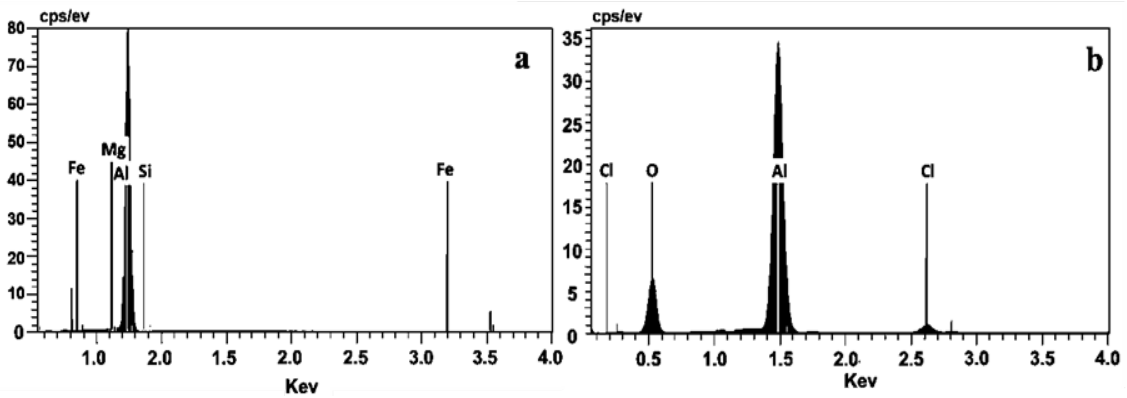

Figure 6. EDX spectra on surface of uncoated Al 6451 (a) before and (b) after corrosion.

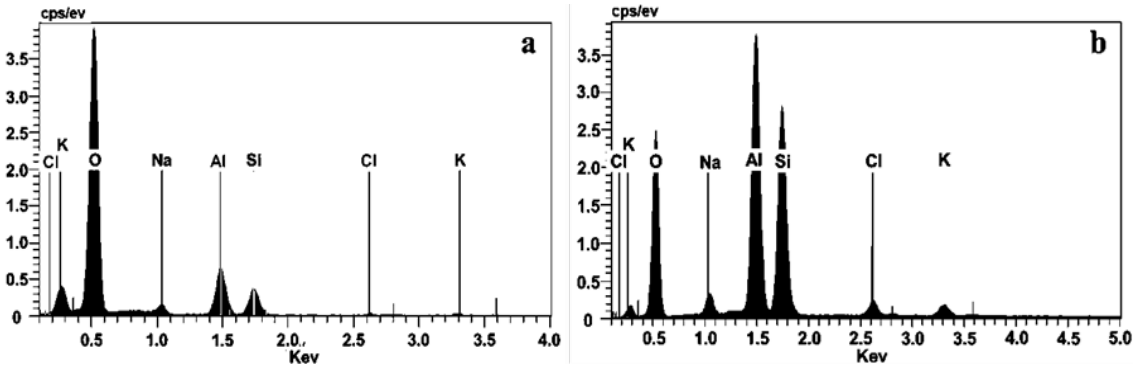

Figure 7. EDX spectra on surface of thin-coated Al 6451 (a) before and (b) after corrosion.

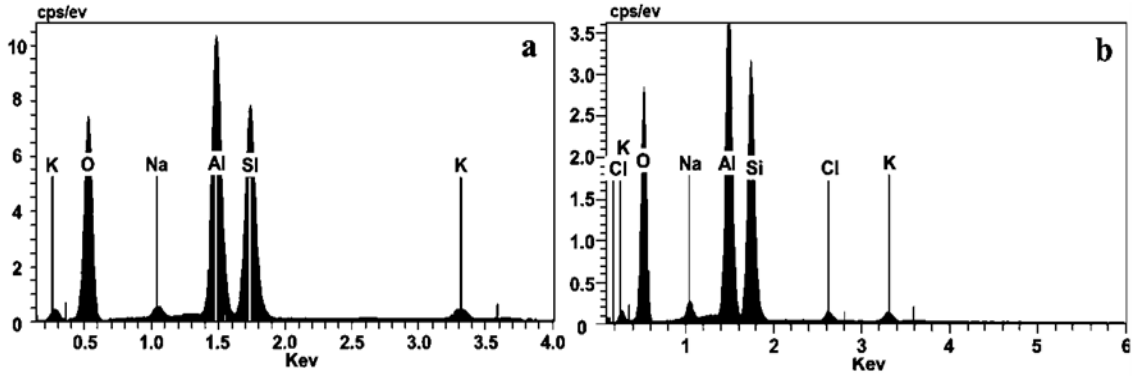

Figure 8. EDX spectra on surface of thick-coated Al 6451 (a) before and (b) after corrosion.

decrease after corrosion tests, although Si was detected in both the thin and thick coatings. To determine the relative Si content, the Al/Si intensity ratios were calculated by the ratio of the intensities of the Al and Si peaks. For the thin coating, the Al/Si intensity ratio decreased from 1.75 before the corrosion test to 1.41 after the test by 22%. The decrease in the Al/Si intensity ratio suggested that some Al was dissolved during the corrosion test. For the thick coating, the Al/Si ratio was reduced from 1.40 before the corrosion test to 1.16 after the test by 17%. The Al/Si ratio reduction for the thick coating was smaller than that of the thin coating. This observation indicated that the thick coating improved the corrosion resistance of Al alloy 6451 more significantly than the thin coating.

4. Summary

By applying a coating layer with the PEO technique, silicate and alumina oxide coatings were deposited on the Al alloy 6451 substrate and formed successive protective films to enhance its corrosion resistance. As the treatment duration increased from 30 s to 90 s, the thickness of coating layer increased by 233%, from 3 μm to 10 μm, the roughness elevated from 1.47 to 3.03. However, after corrosion testing, an electrochemical polishing mechanism could be observed due to the roughness decrease, which was 1.33 and 2.88, respectively. The variation of the surface morphologies of the coatings was verified with the SEM analyses. The results of the potentiodynamic polarization tests indicated that the corrosion resistances of the uncoated, thin-coated and thick-coated Al 6451 were 7282.5 $\Omega \cdot cm^2$, 11583.3 $\Omega \cdot cm^2$ and 41,151 $\Omega \cdot cm^2$, respectively, indicating the growth of coating layer enhanced the ability of the substrate combating with corrosive environment significantly. From the EDX spectra, the reduction in the calculated Al/Si intensity ratio before and after corrosion tests for the thick coating was smaller than that of the thin coating, indicating that the thick coating improved the corrosion resistance of Al alloy 6451 more significantly than the thin coating.

Acknowledgements

The authors extend their gratitude to the Natural Sciences and Engineering Research Council of Canada (NSERC) and the University of Windsor for supporting the work.

Conflicts of Interest

The authors declare no conflicts of interest regarding the publication of this paper.

References

[1] (2024) The 2024 EPA Automotive Trends Report—Greenhouse Gas Emissions, Fuel Economy, and Technology since 1975, EPA-420-R-24-022. U.S. Environmental Protection Agency.

[2] Zheng, Y., Li, J., Shen, W., Zhang, T., Hu, H. and Nie, X. (2026) Effect of PEO Coating on Mechanical Properties of Stamped Wrought Al 6451 Alloy. *Materialwissenschaft*

und Werkstofftechnik, e70090. https://doi.org/10.1002/mawe.70090

[3] Shen, W., Hu, A., Liu, S. and Hu, H. (2023) Al-MN Alloys for Electrical Applications: A Review. *Journal of Alloys and Metallurgical Systems*, **2**, Article ID: 100008. https://doi.org/10.1016/j.jalmes.2023.100008

[4] Li, Y., Hu, A., Fu, Y., Liu, S., Shen, W., Hu, H., et al. (2022) Al Alloys and Casting Processes for Induction Motor Applications in Battery-Powered Electric Vehicles: A Review. *Metals*, **12**, Article 216. https://doi.org/10.3390/met12020216

[5] Liu, S.F., Hu, A., Hu, H., Nie, X. and Kar, N.C. (2022) Potential Al-Fe Cast Alloys for Motor Applications in Electric Vehicles: An Overview. *Key Engineering Materials*, **923**, 3-19. https://doi.org/10.4028/p-3027xi

[6] Davis, J.R. (2002) Aluminum and Aluminum Alloys-ASM Specialty Handbook. ASM International, 645 p.

[7] Taub, A., De Moor, E., Luo, A., Matlock, D.K., Speer, J.G. and Vaidya, U. (2019) Materials for Automotive Lightweighting. *Annual Review of Materials Research*, **49**, 327-359. https://doi.org/10.1146/annurev-matsci-070218-010134

[8] Taub, A.I. and Luo, A.A. (2015) Advanced Lightweight Materials and Manufacturing Processes for Automotive Applications. *MRS Bulletin*, **40**, 1045-1054. https://doi.org/10.1557/mrs.2015.268

[9] Hao, Y., Ye, Z., Ye, M., Dong, H., Wang, L. and Du, Y. (2023) Construction and Growth of Black PEO Coatings on Aluminum Alloys for Enhanced Wear and Impact Resistance. *Ceramics International*, **49**, 30782-30793. https://doi.org/10.1016/j.ceramint.2023.07.034

[10] Giampieri, A., Ling-Chin, J., Ma, Z., Smallbone, A. and Roskilly, A.P. (2020) A Review of the Current Automotive Manufacturing Practice from an Energy Perspective. *Applied Energy*, **261**, Article ID: 114074. https://doi.org/10.1016/j.apenergy.2019.114074

[11] Tait, W.S. (2013) Corrosion Prevention and Control of Chemical Processing Equipment. In: Kutz, M., Ed., *Handbook of Environmental Degradation of Materials*, Elsevier, 863-886.

[12] Sukiman, N.L., Zhou, X., Birbilis, N., Hughes, A.E., Mol, J.M.C., Garcia, S.J., Zhou, X. and Thompson, G.E. (2012) Durability and Corrosion of Aluminium and Its Alloys: Overview, Property Space, Techniques and Developments. In: Ahmad, Z., Ed., *Aluminium Alloys—New Trends in Fabrication and Applications*, InTech, 16-27. https://www.intechopen.com/chapters/41099

[13] Khan, A.A., Razin, A.A., Ahammed, D.S. and Kaiser, M.S. (2023) Comparison of Electrochemical Corrosion Performance of Eutectic Al-Si Automotive Alloy in Deep Seawater and 3.5% NaCl Solution. *Materials Today*: *Proceedings*, **82**, 241-247. https://doi.org/10.1016/j.matpr.2023.01.179

[14] Dumitrascu, V., Benea, L. and Danaila, E. (2017) Corrosion Behavior of Aluminum Oxide Film Growth by Controlled Anodic Oxidation. *IOP Conference Series*: *Materials Science and Engineering*, **209**, Article ID: 012016. https://doi.org/10.1088/1757-899x/209/1/012016

[15] Graedel, T.E. (1989) Corrosion Mechanisms for Aluminum Exposed to the Atmosphere. *Journal of The Electrochemical Society*, **136**, 204C-212C. https://doi.org/10.1149/1.2096869

[16] Abdul, M., Shen, W., Ying, L. and Hu, H. (2024) Corrosion Effect on Mechanical Properties of Stamped Al Alloy 6451 for Auto Applications. In: Wagstaff, S., Ed., *Light Metals* 2024, Springer, 165-170. https://doi.org/10.1007/978-3-031-50308-5_20

[17] Sikdar, S., Menezes, P.V., Maccione, R., Jacob, T. and Menezes, P.L. (2021) Plasma Electrolytic Oxidation (PEO) Process—Processing, Properties, and Applications. *Nanomaterials*, **11**, Article 1375. https://doi.org/10.3390/nano11061375

[18] Seshan, K. (2001) Handbook of Thin Film Deposition. William Andrew, 28-40.

[19] ASTM standard A1093/A1093M-15 (2020) Standard Specification for Electrolytic Plasma Treatment Processing of Conductive Materials. ASTM Standards.

[20] Hu, A., Geng, X., Hu, H. and Nie, X. (2025) Corrosion Resistance of Squeeze Cast Magnesium Alloy AM60-Based Hybrid Nanocomposite Coated with Plasma Electrolytic Oxidation. *Advances in Materials and Processing Technologies*, **11**, 798-817. https://doi.org/10.1080/2374068x.2024.2335705

[21] Ma, Y., Hu, H., Northwood, D. and Nie, X. (2007) Optimization of the Electrolytic Plasma Oxidation Processes for Corrosion Protection of Magnesium Alloy AM50 Using the Taguchi Method. *Journal of Materials Processing Technology*, **182**, 58-64. https://doi.org/10.1016/j.jmatprotec.2006.07.007